Journal of Sound and Vibration (1998) **218**(5), 799–823
Article No. sv981834

SOUND PROPAGATION OVER NOISE BARRIERS WITH ABSORBING GROUND

D. Duhamel and P. Sergent

Ecole Nationale des ponts et chaussées, *CERAM*, 6 *et* 8 *Avenue Blaise Pascal*, *Cité Descartes*, *Champs-sur-Marne*, 77455 *Marne-La-Vallée Cedex* 2, *France*

(*Received* 13 *October* 1997, *and in final form* 24 *June* 1998)

The main purpose of this article is to present a numerical method for calculating the sound pressure around noise barriers of arbitrary geometry. Varying impedance boundary conditions on the barrier and constant impedance on the ground are assumed. Sound propagation over an infinite barrier with a constant cross-section for an harmonic point source is determined by solving 2D problems only, avoiding the computational complexity of the solution of a true 3D problem. This can be done by using the solutions of a set of 2D models for a coherent line source for real and *imaginary* wavenumbers. This extension to calculations for *imaginary* wavenumbers is the main feature of the proposed method. A Fourier transform of the 2D solutions allows a calculation of the 3D solution for a point source. The 2D numerical solutions are obtained by a classical use of the Boundary Element Method. Moreover, the 2D Green function for *imaginary* wavenumbers in the case of a half-space bounded by a surface of uniform impedance is developed. Finally, examples are given to estimate the accuracy of the method and some practical cases of calculations around barriers are presented and compared with experimental data.

1. INTRODUCTION

A usual practical problem found in outdoor noise propagation is the calculation of the sound pressure around a noise barrier built over an absorbing ground. Approximate values of the pressure can be given by analytical or geometrical acoustic solutions for simple cases. However to get precise results, especially in the case of complex geometrical shapes, one turns to numerical methods. For a quiescent atmosphere under uniform temperature conditions, the sound propagation is governed by the Helmholtz equation. This equation can be solved by different means but, as the domain has an infinite extent, one of the most popular approaches is the Boundary Element Method (BEM). For instance Seznec [1] and Hothersall [2, 3] have solved two-dimensional diffraction problems by the BEM for rigid barriers above a rigid plane in the former and absorbing barriers above an impedance plane in the latter. In this case the sound pressure is supposed to be created by a coherent line source and is calculated on a cross-section of the barrier. These calculations give important insights into the physical phenomenon

0022–460X/98/500799 + 25 $30.00/0

and allow a comparison of the efficiencies of different shapes of barriers. They do not give, however, the full three-dimensional picture of the sound pressure around a noise barrier.

Kawai and Terai [4] and Antes [5] have extended the calculations to three-dimensional problems and sound pressures created by point sources above a rigid plane. In their BEM code they discretise the two-dimensional surface of a finite part of the barrier and solve the corresponding discrete problem. Because of the large computational cost required by the solution of the 3D problem, the pressure can only be reasonably calculated for low frequencies and for barriers of small lengths. Otherwise the calculation cost becomes rapidly prohibitive. For instance the practical case of a barrier of 20 m length diffracting the pressure created by a point source at the frequency 1000 Hz would be very difficult to solve with the previous methods.

To overcome this problem, a method was presented by Duhamel [6, 7] to calculate the sound pressure created by a point source and diffracted by a barrier of infinite length and uniform cross-section located over rigid ground. It is proved that if the 2D spectrum for real and *imaginary* wavenumbers is calculated, a Fourier transform can then provide the full three-dimensional pressure at every point outside the barrier, not only in the plane containing the point source. The model can be further extended to the calculation of incoherent line sources. The purpose of this paper is to extend this method to the important practical case of barriers built over flat ground with homogeneous impedance.

If discretisation of the ground is to be avoided for BEM calculations with impedance grounds, the Green function must be determined. This formulation was performed in the two-dimensional case by Hothersall *et al*. [2] who solved the Helmholtz equation by the BEM for a sound pressure created by a coherent line source above a plane with an admittance boundary condition. Contrary to a rigid boundary condition where the Green function is simple and well known, the Green function for an impedance boundary condition is much more difficult to calculate.

For a point source above a plane boundary with uniform impedance, an exact solution has been given by Ingard [8], Wenzel [9] and Thomasson [10]. The solution of Thomasson is an integral in a form suitable for numerical calculations. Numerous approximate solutions with various degrees of accuracy were also derived by Wenzel [9], Chien and Soroka [11, 12], Thomasson [13], Kawai *et al*. [14], Nobile and Hayek [15] and Li *et al*. [16]. The Green function for a coherent line source was obtained by Chandler-Wilde and Hotehersall [17] and in an efficient form for numerical calculations in reference [18]. An approximate formula was obtained by Li *et al*. [16].

These results will be used to obtain the two-dimensional solutions for coherent line sources. Furthermore, they must be extended to obtain the solutions for *imaginary* wavenumbers which are required in the proposed method. After applying a Fourier transformation a real sound pressure in a 3D model is realized. Thus, the sound pressure created by a point source around a barrier of constant cross-section may be determined. This pressure can be calculated in the whole domain outside the barrier, not only in the section containing the point source.

The paper is organized as follows. Section 2 presents the main features of the method transforming the 2D solutions to get 3D results independently of the numerical tool used to solve the Helmholtz equation. In section 3 a boundary element method is formulated for solving the 2D problems. In section 4 the two-dimensional Green function is calculated with a special emphasis on complex wavenumbers which do not seem to have been studied before. In section 5 the 2D to 3D transformation is tested for the case of a point source in a half-space, the only case for which analytical results are available. Finally, in section 6 the numerical results are compared to other computational methods and to experimental data.

2. TRANSFORMATION FROM 2D TO 3D

The problem consists of solving the Helmholtz equation in a three-dimensional domain exterior to a noise barrier above a ground surface with a locally reacting homogeneous acoustic admittance. The present method is to be used for barriers of constant cross-section, which means that the cross-section can be arbitrarily chosen but we suppose that it does not change along its length. A typical example is shown in Figure 1 where the T shape does not change in the y direction. Suppose that the sound pressure is excited by a point source in the fluid domain which generates, in free field, the pressure $e^{iKr}/(4\pi r)$ with the time dependence $e^{-i\omega t}$ suppressed throughout, where ω is the angular frequency, c the speed of sound and $K = \omega/c$ the wavenumber.

The principle of the transformation from 2D to 3D starts from the following relation where the pressure of a 3D point source is calculated from the summation of fields of two-dimensional sources by the Fourier transform (reference [19], formula 6.616)

$$-2i\frac{e^{iK\sqrt{r^2+y^2}}}{\sqrt{r^2+y^2}} = \int_{-\infty}^{+\infty} H_0^{(1)}(r\sqrt{K^2-t^2})\, e^{ity}\, dt, \tag{1}$$

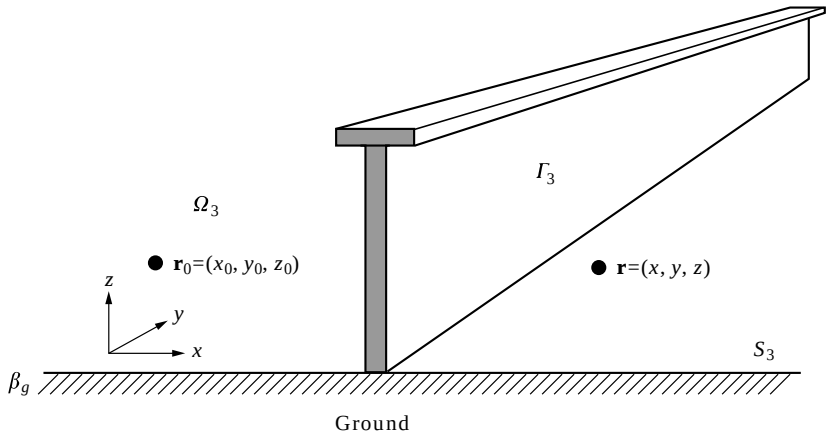

Figure 1. Noise barrier of constant cross-section with Ω_3 the 3D fluid domain, Γ_3 the barrier surface, S_3 the ground surface, β_g the ground admittance, $\mathbf{r}_0$ the source point and $\mathbf{r}$ the observation point.

where $0 \leqslant \arg(\sqrt{K^2 - t^2}) < \pi$ and $r = \sqrt{x^2 + z^2} > 0$ is the radial distance in the (x, z) plane between the observation point and the source. Multiplying both sides of the equality by $i/8\pi$, the left hand side becomes $e^{iK}\sqrt{r^2 + y^2}/4\pi\sqrt{r^2 + y^2}$ the sound pressure due to a 3D point source while the right hand side appears as the Fourier transform of $i/4H_0^{(1)}(r\sqrt{K^2 - t^2})$, the sound pressure due to a line source with wavenumber $\sqrt{K^2 - t^2}$ which can take imaginary values. For imaginary values of the variable and $u > 0$, $i/4H_0^{(1)}(iu) = 1/2\pi K_0(u)$ where K_0 is the modified Bessel function of zero order. Relation (1) for point sources in free field will be extended to solutions of diffraction problems and the solutions of 3D problems will be calculated as Fourier transforms of solutions to 2D problems.

To take into account the diffraction by the barrier and the reflection on the ground the pressure, p, is the solution to the following problem:

$$\Delta p + K^2 p = -\delta(\mathbf{r} - \mathbf{r_0}) \quad \text{in} \quad \Omega_3, \tag{2}$$

$$\frac{\partial p}{\partial n} + iK\beta_s p = 0 \quad \text{on} \quad \Gamma_3, \tag{3}$$

$$\frac{\partial p}{\partial z} + iK\beta_g p = 0 \quad \text{on} \quad S_3, \tag{4}$$

$$\frac{\partial p}{\partial r} - iKp = o\left(\frac{1}{r}\right), \tag{5}$$

$$p = o\left(\frac{1}{r}\right). \tag{6}$$

Here p is the complex amplitude of the pressure, $K = \omega/c$ is the wavenumber, $\mathbf{r_0}$ is the position of the point source of sound, $\mathbf{r} = (x, y, z)$ with $z > 0$ as the observation point and Ω_3 is the 3D domain outside the barrier. Relation (3) is the boundary condition on the barrier of surface Γ_3 with a surface admittance β_s which is a function of the boundary point, relation (4) is the boundary condition on the ground of surface S_3 with a constant admittance β_g and relations (5) and (6) are the Sommerfeld radiation conditions at infinity. According to the limiting absorption principle [20], the solution is also the limit when $v \to 0$ of solutions of problem (2–6) for complex wavenumbers $\tilde{K}$ such that $\tilde{K}^2 = K^2 + iv$.

As a consequence of the invariance of the geometry in the y direction one can take the Fourier transform of the pressure in the y variable. With an explicit dependence on the admittances β_s and β_g and noting k_y the variable in the wavenumber domain, this is given by

$$\hat{p}(x, k_y, z, \beta_s, \beta_g) = \int_{-\infty}^{+\infty} p(x, y, z, \beta_s, \beta_g)\, e^{ik_y y}\, dy. \tag{7}$$

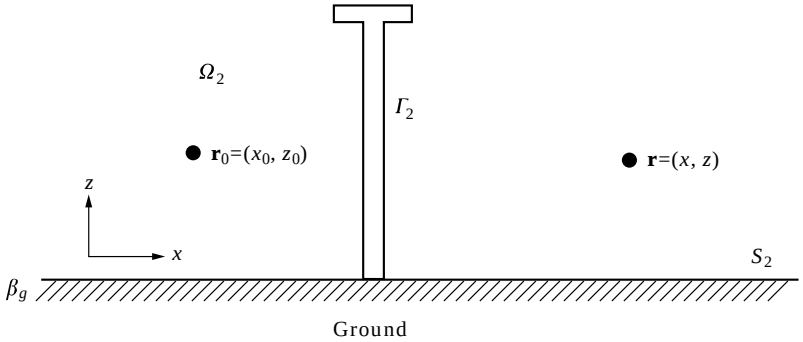

Figure 2. 2D problem on a cross-section with Ω_2 the 2D fluid domain, Γ_2 the barrier surface, S_2 the ground surface, β_g the ground admittance, $\mathbf{r}_0$ the source point and $\mathbf{r}$ the observation point.

From the 3D problem satisfied by the pressure p it can easily be shown that the Fourier transform $\hat{p}$ is the solution of the following problem:

$$\Delta\hat{p} + (K^2 - k_y^2)\hat{p} = -e^{ik_y y_0}\delta(x - x_0)\delta(z - z_0) \quad \text{in} \quad \Omega_2, \tag{8}$$

$$\frac{\partial\hat{p}}{\partial n} + iK\beta_s\hat{p} = 0 \quad \text{on} \quad \Gamma_2, \tag{9}$$

$$\frac{\partial\hat{p}}{\partial z} + iK\beta_g\hat{p} = 0 \quad \text{on} \quad S_2. \tag{10}$$

The problem is now posed on a 2D cross-section only with the corresponding boundaries and boundary conditions on the solution (see Figure 2). This 2D problem consists of finding the pressure at (x, z) created by a line source at the position (x_0, z_0) around a cross-section of the barrier. The only difference with the usual problem is that the wavenumber $k = \sqrt{K^2 - k_y^2}$ can take imaginary values when $K^2 - k_y^2 < 0$.

This problem will be related to the solution of the following set of classical 2D problems.

$$\Delta q + k^2 q = -\delta(x - x_0)\delta(x - z_0) \quad \text{in} \quad \Omega_2, \tag{11}$$

$$\frac{\partial q}{\partial n} + ik\beta_s q = 0 \quad \text{on} \quad \Gamma_2, \tag{12}$$

$$\frac{\partial q}{\partial z} + ik\beta_g q = 0 \quad \text{on} \quad S_2, \tag{13}$$

$$\frac{\partial q}{\partial r} - ikq = o\left(\frac{1}{\sqrt{r}}\right), \tag{14}$$

$$q = o\left(\frac{1}{\sqrt{r}}\right). \tag{15}$$

where k is a real number or a purely imaginary number with a positive imaginary part. For real wavenumbers k this is a classical problem with impedance boundary

conditions. For complex wavenumbers k such that $\mathrm{Im}\,(k) > 0$ the problem has a unique solution because the frequencies for which the problem (11–15) does not possess a unique solution are known to belong to the lower part of the complex plane where $\mathrm{Im}\,(k) < 0$ [20]. When k is complex with $\mathrm{Im}\,(k) > 0$ the solution is in fact exponentially decreasing for large r. In the following section a numerical method based on the Boundary Element Method will be extended for *imaginary* wavenumbers. The solution of the problem (11–15) at the observation point (x, z) for the complex wavenumber k and the normalized admittances β_s and β_g on the barrier and on the ground, respectively, will be noted by $q(x, k, z, \beta_s, \beta_g)$ in the following.

The comparison of formulae (8–10) with (11–15) shows that the Fourier transform solution $\hat{p}$ of the 3D problem can be expressed with respect to the previous 2D problem. We are now in a position to formulate the solution of the original 3D problem, equations (2–6). Suppose that the previous problem (11–15) has been solved for k in the interval $[0, K]$ and along the imaginary axis, the solution of the 3D problem, equations (2–6), may be recovered by the following formula which is essentially an inverse Fourier transform,

$$p(x, y, z) = \frac{1}{2\pi} \int_{-\infty}^{+\infty} q(x, \sqrt{K^2 - k_y^2}, z, \beta_s/\sqrt{1 - k_y^2/K^2}, \beta_g/\sqrt{1 - k_y^2/K^2}) \times \mathrm{e}^{-\mathrm{i}k_y(y - y_0)}\, \mathrm{d}k_y . \tag{16}$$

where the square root is taken with the conditions

$$\mathrm{Re}\,(\sqrt{1 - k_y^2/K^2}) \geqslant 0, \qquad \mathrm{Im}\,(\sqrt{1 - k_y^2/K^2}) \geqslant 0.$$

When $K^2 - k_y^2$ is positive the 2D solution is calculated for the real wavenumber $k = \sqrt{K^2 - k_y^2}$, whereas when $K^2 - k_y^2$ is negative the solution is calculated for the *imaginary* wavenumber $k = \mathrm{i}\sqrt{k_y^2 - K^2}$. More precisely one must calculate for real wavenumbers in the interval $[0, K]$ and on the imaginary axis. In the latter case the solution is exponentially decreasing as a function of k_y, so only a limited range is needed.

To estimate the number of calculations, observe that the 2D solution for real wavenumbers oscillates approximately like $\mathrm{e}^{\mathrm{i}kr}$ where r is the distance between the source and the receiver. This fact can be explained by calculating the incident pressure $\mathrm{i}/4\mathrm{H}_0^{(1)}(kr)$ or the scattered pressure in far field. Le r_{max} be the maximum distance of interest. The oscillations of the function are well estimated by taking five points per period. This means that the sound pressure must be calculated for wavenumbers in the interval $[0, K]$ with a spacing between two successive wavenumbers of order

$$\Delta k = \frac{2\pi}{5 r_{max}} . \tag{17}$$

Here the maximum number of calculations required for a 3D solution at a frequency ω is, in the real frequency domain

$$n = \frac{\omega}{\Delta\omega} = \frac{k}{\Delta k} = 5\,\frac{r_{max}}{\lambda}\,. \tag{18}$$

With approximately an equal number of points for the *imaginary* wavenumbers, the number of frequency points is approximately

$$n_f = 10\,\frac{r_{max}}{\lambda}\,. \tag{19}$$

So a calculation for a larger distance requires a denser frequency sampling.

One must notice another point concerning the number of 2D solutions required to calculated the 3D sound pressure for several frequencies. When the boundaries are rigid, we calculate the 2D solutions for real and *imaginary* wavenumbers and from this set of solutions it is possible to obtain the 3D sound pressure for different frequencies [6, 7]. For the admittance boundary condition, the number of calculations is larger. To obtain the sound pressure for the wavenumber K, the 2D solutions $q(x, \sqrt{K^2 - k_y^2}, z, \beta_s/\sqrt{1 - k_y^2/K^2}, \beta_g/\sqrt{1 - k_y^2/K^2})$ are required. But this set of solutions cannot be used for another wavenumber $K' \neq K$. On the contrary another full set of 2D solutions $q(x, \sqrt{K'^2 - k_y^2}, z, \beta_s/\sqrt{1 - k_y^2/K'^2}, \beta_g/\sqrt{1 - k_y^2/K'^2})$ is necessary.

This method makes possible three-dimensional calculations for medium and high frequencies. Notice that the previous expressions do not make assumptions on the method for solving the boundary value problem. Hence, analytical techniques may be used. The following section describes a numerical method for solving the Helmholtz equation.

3. NUMERICAL SOLUTION OF 2D PROBLEMS

To complete the analysis we need a numerical method to solve the 2D problem (11–15) for any cross-section. The classical boundary element method is used here. The sound pressure satisfies the following boundary integral equation

$$c(\mathbf{x})q(\mathbf{x}) = q_{inc}(\mathbf{x}) + \int_{\partial\Omega} q(\mathbf{y})\,\frac{\partial G}{\partial \mathbf{n}_y}\,(\mathbf{y}, \mathbf{x})\,\mathrm{d}\mathbf{y} - \int_{\partial\Omega} \frac{\partial q}{\partial \mathbf{n}_y}\,(\mathbf{y})G(\mathbf{y}, \mathbf{x})\,\mathrm{d}\mathbf{y} \tag{20}$$

and taking account of the boundary condition on the barrier this yields

$$c(\mathbf{x})q(\mathbf{x}) = q_{inc}(\mathbf{x}) + \int_{\partial\Omega} q(\mathbf{y}) \left(\frac{\partial G}{\partial \mathbf{n}_y}\,(\mathbf{y}, \mathbf{x}) + \mathrm{i}k\beta_s(\mathbf{y})G(\mathbf{y}, \mathbf{x}) \right) \mathrm{d}\mathbf{y}, \tag{21}$$

where $c(\mathbf{x}) = \theta(x)/2\pi$ on the boundary and θ is the angle inside the fluid domain of the two tangents at point $\mathbf{x}$ (see Figure 3). This coefficient can also be calculated by the formula

$$c(\mathbf{x}) = 1 + \int_{\partial\Omega} \frac{\partial g_0}{\partial \mathbf{n}_y}\,(\mathbf{y}, \mathbf{x})\,\mathrm{d}\mathbf{y}, \tag{22}$$

where g_0 is the Green function solution of $\Delta_y g_0(\mathbf{y}, \mathbf{x}) = -\delta(\mathbf{y} - \mathbf{x})$ in the upper half-space with a rigid boundary condition on the ground and is given by

$$g_0(\mathbf{y}, \mathbf{x}) = -\frac{1}{2\pi} \log(R) - \frac{1}{2\pi} \log(R'). \tag{23}$$

The distances are defined as $R = |\mathbf{x} - \mathbf{y}|$ and $R' = |\mathbf{x} - \mathbf{y}'|$ where $\mathbf{y}$ is the source point, $\mathbf{y}'$ is the image source with respect to the ground and $\mathbf{x}$ is the observation point.

The Green function with admittance boundary condition G is given in the next section. q_{inc} is the incident pressure created by sources in the half-space without barrier. In case of a unit point source at point $\mathbf{x}_0$, its value is given by

$$q_{inc}(\mathbf{x}) = G(\mathbf{x}, \mathbf{x}_0). \tag{24}$$

For the numerical solution of equation (20) we divide the boundary into a number of quadratic elements (with three nodes) for better precision. The integral on the boundary is divided into N elements by

$$c(\mathbf{x})q(\mathbf{x}) = q_{inc}(\mathbf{x}) + \sum_{i=1}^{N} \int_{\Gamma_i} q(\mathbf{y}) \left(\frac{\partial G}{\partial \mathbf{n}_y}(\mathbf{y}, \mathbf{x}) + \mathrm{i}k\beta_s(\mathbf{y}) G(\mathbf{y}, \mathbf{x}) \right) \mathrm{d}\mathbf{y}. \tag{25}$$

In each element the pressure is interpolated by

$$q(\xi) = q_1 N_1(\xi) + q_2 N_2(\xi) + q_3 N_3(\xi), \tag{26}$$

where the q_i are the nodal values of the pressure inside the element, ξ is the local variable defined on the interval $[-1, 1]$ and N_i are the interpolation functions given below

$$N_1(\xi) = \frac{\xi}{2}(\xi - 1), \qquad N_2(\xi) = 1 - \xi^2, \qquad N_3(\xi) = \frac{\xi}{2}(1 + \xi). \tag{27}$$

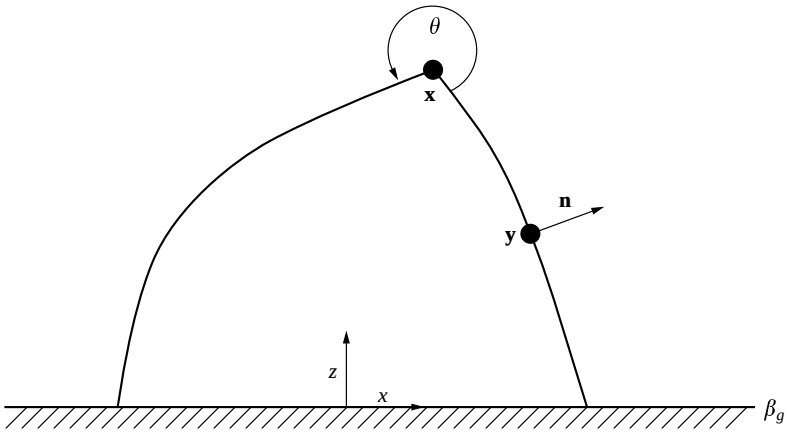

Figure 3. 2D domain of arbitrary section with **x** the collocation point, **y** the source point, **n** the normal at **y** and θ the angle in the fluid domain at point x.

Then the following integrals

$$\int_{-1}^{1} \left(\frac{\partial G}{\partial \mathbf{n}_y} (\mathbf{y}(\xi), \mathbf{x}) + \mathrm{i}k\beta_s(\mathbf{y}(\xi)) G(\mathbf{y}(\xi), \mathbf{x}) \right) |\mathbf{y}'(\xi)| N_j(\xi)\, \mathrm{d}\xi \tag{28}$$

are evaluated numerically by Gauss integration with three points for elements far from the collocation point and seven points on the singular element. In this latter case a change of variable $\xi \to \xi^2$ in the vicinity of the collocation point is used to cancel the logarithmic singularity.

Writing relation (25) for the nodal points, one obtains a linear system. The solution of this system gives the pressure at the nodal points. For other boundary points the pressure is calculated by formula (26) and for points inside the fluid domain by formula (20).

4. 2D GREEN FUNCTIONS

Now the expression for the Green function in a half-space with an admittance boundary condition must be determined. This function $G(\mathbf{r}, \mathbf{r}_0)$ gives the pressure at point $\mathbf{r}$ created by a line source at point $\mathbf{r}_0$. For real wavenumbers it is the solution of the following mathematical problem

$$\Delta G(\mathbf{r}, \mathbf{r}_0) + k^2 G(\mathbf{r}, \mathbf{r}_0) = -\delta(\mathbf{r} - \mathbf{r}_0), \tag{29}$$

$$\frac{\partial G}{\partial z} (\mathbf{r}, \mathbf{r}_0) + \mathrm{i}k\beta_g G(\mathbf{r}, \mathbf{r}_0) = 0 \quad \text{on} \quad S_2, \tag{30}$$

$$\frac{\partial G}{\partial n} (\mathbf{r}, \mathbf{r}_0) - \mathrm{i}k G(\mathbf{r}, \mathbf{r}_0) = o\left(\frac{1}{\sqrt{r}} \right), \tag{31}$$

$$G(\mathbf{r}, \mathbf{r}_0) = o\left(\frac{1}{\sqrt{r}} \right). \tag{32}$$

It is traditional to write this Green function as

$$G(\mathbf{r}, \mathbf{r}_0) = G_0(\mathbf{r}, \mathbf{r}_0) + P(\mathbf{r}, \mathbf{r}_0), \tag{33}$$

where G_0 is the solution for a rigid boundary condition given by

$$G_0(\mathbf{r}, \mathbf{r}_0) = \frac{\mathrm{i}}{4} \mathrm{H}_0^{(1)}(kR) + \frac{\mathrm{i}}{4} \mathrm{H}_0^{(1)}(kR'), \tag{34}$$

where $\mathrm{H}_0^{(1)}$ is the Hankel function. The function $P(\mathbf{r}, \mathbf{r}_0)$ is the corrective term coming from the admittance boundary condition. Some comments on the evaluation of this function can be found in Appendix A.

The case of finding P for an *imaginary* wavenumber ($\mathrm{i}k$) can be found by analytic continuation of P in (56). Writing the Green function as the Green

function with rigid boundary condition plus a correction term as in relation (33), this term is the solution of

$$\Delta P(\mathbf{r}, \mathbf{r}_0) - k^2 P(\mathbf{r}, \mathbf{r}_0) = 0, \tag{35}$$

$$\frac{\partial P}{\partial z}(\mathbf{r}, \mathbf{r}_0) - k\beta_g P(\mathbf{r}, \mathbf{r}_0) = \frac{k\beta_g}{\pi} \mathrm{K}_0(k|\mathbf{r} - \mathbf{r}_0|) \quad \text{on} \quad S_2, \tag{36}$$

$$P(\mathbf{r}, \mathbf{r}_0) = o\left(\frac{1}{\sqrt{r}}\right). \tag{37}$$

where K_0 is the modified Bessel function of order zero through the relation $\mathrm{i}/4\mathrm{H}_0^{(1)}(\mathrm{i}ku) = 1/2\pi\mathrm{K}_0(ku)$.

Taking the Fourier transform of P in the variable x, this yields

$$\hat{P}(k_x, z, x_0, z_0) = \int_{-\infty}^{+\infty} P(x, z, x_0, z_0)\, \mathrm{e}^{\mathrm{i}k_x x}\, \mathrm{d}x. \tag{38}$$

This function is the solution of

$$\frac{\mathrm{d}^2 P}{\mathrm{d}z^2} - (k^2 + k_x^2)\hat{P} = 0,$$

$$\frac{\mathrm{d}\hat{P}}{\mathrm{d}z}(k_x, 0, x_0, z_0) - k\beta_g \hat{P}(k_x, 0, x_0, z_0) = \frac{k\beta_g}{\pi} \int_{-\infty}^{+\infty} \mathrm{K}_0(k\sqrt{(x - x_0)^2 + z_0^2})\, \mathrm{e}^{\mathrm{i}k_x x}\, \mathrm{d}x,$$

$$= \frac{k\beta_g}{\sqrt{k^2 + k_x^2}}\, \mathrm{e}^{\mathrm{i}k_x x_0}\, \mathrm{e}^{-z_0\sqrt{k^2 + k_x^2}}. \tag{39}$$

The last relation comes from Gradshteyn formula (6.677) (reference [19], number 5, p. 736). Taking the inverse Fourier transform and making the change of variable $k_x = ks$ one gets

$$P(x, z, x_0, z_0) = -\frac{\beta_g}{2\pi} \int_{-\infty}^{+\infty} \frac{\mathrm{e}^{k[-(z + z_0)\sqrt{1 + s^2} + \mathrm{i}s(x_0 - x)]}}{\sqrt{1 + s^2}(\beta_g + \sqrt{1 + s^2})}\, \mathrm{d}s. \tag{40}$$

For a better computational efficiency this expression is transformed by

$$P(x, z, x_0, z_0) = -\frac{\beta_g}{\pi} \int_0^{+\infty} \frac{\mathrm{e}^{-k(z + z_0)\sqrt{1 + s^2}} \cos(ks(x - x_0))}{\sqrt{1 + s^2}(\beta_g + \sqrt{1 + s^2})}\, \mathrm{d}s$$

$$= -\frac{\beta_g}{\pi} \int_1^{+\infty} \frac{\mathrm{e}^{-k(z + z_0)t} \cos(k(x - x_0)\sqrt{t^2 - 1})}{\sqrt{t^2 - 1}(\beta_g + t)}\, \mathrm{d}t$$

$$= -\frac{\beta_g}{\pi}\, \mathrm{e}^{-k(z + z_0)} \int_0^{+\infty} \mathrm{e}^{-k(z + z_0)u} \frac{h(u)}{\sqrt{u}}\, \mathrm{d}u, \tag{41}$$

with

$$h(u) = \frac{\cos\left(k(x - x_0)\sqrt{u(u+2)}\right)}{\sqrt{u+2}(\beta_g + 1 + u)}. \tag{42}$$

When $\alpha = k(z + z_0) > 0$, the expression (41) can be calculated by Gauss–Laguerre numerical integration which is especially adapted to the weight $1/\sqrt{u}$. The implemented formula is

$$P(x, z, x_0, z_0) = -\frac{\beta_g}{\pi}\frac{e^{-\alpha}}{\sqrt{\alpha}}\int_0^{+\infty}\frac{e^{-v}h(v/\alpha)}{\sqrt{v}}\,dv, \tag{43}$$

with 10 points of integration. When $k(x + z_0)$ equals zero or takes a small value, one can still integrate numerically the formula (41) but with less efficiency by subdividing the integral over [0, 1] and [1, ∞]. The latter is calculated by the change of variable $u \to 1/u$ and a Gauss-formula on [0, 1].

In the BEM method one also needs the derivative of the Green function. Taking the formula (40) and differentiating under the integral, this yields

$$\frac{\partial P}{\partial x}(x, z, x_0, z_0) = \frac{ik\beta_g}{2\pi}\int_{-\infty}^{+\infty} s\,\frac{e^{k[-(z+z_0)\sqrt{1+s^2} + is(x_0 - x)]}}{\sqrt{1+s^2}(\beta_g + \sqrt{1+s^2})}\,ds. \tag{44}$$

Transformations similar to (41) yield

$$\frac{\partial P}{\partial x}(x, z, x_0, z_0) = \operatorname{sign}(x - x_0)\frac{k\beta_g}{\pi}\frac{e^{-\alpha}}{\alpha}\int_0^{+\infty} e^{-v}g(v/\alpha)\,dv, \tag{45}$$

with

$$g(v) = \frac{\sin\left(k|x - x_0|\sqrt{v(v+2)}\right)}{\beta_g + 1 + v}. \tag{46}$$

The exponential term allows a numerical integration by techniques similar to that used for formula (43). The derivative with respect to z is given by

$$\begin{aligned}\frac{\partial P}{\partial z}(x, z, x_0, z_0) &= -\frac{\beta_g}{2\pi}\int_{-\infty}^{+\infty} -k\sqrt{1+s^2}\,\frac{e^{k[-(z+z_0)\sqrt{1+s^2} + is(x_0 - x)]}}{\sqrt{1+s^2}(\beta_g + \sqrt{1+s^2})}\,ds \\ &= \frac{\beta_g k}{2\pi}\int_{-\infty}^{+\infty}\frac{e^{k[-(z+z_0)\sqrt{1+s^2} + is(x_0 - x)]}}{\sqrt{1+s^2}}\,ds \\ &\quad + k\beta_g\left\{-\frac{\beta_g}{2\pi}\int_{-\infty}^{+\infty}\frac{e^{k[-(z+z_0)\sqrt{1+s^2} + is(x_0 - x)]}}{\sqrt{1+s^2}(\beta_g + \sqrt{1+s^2})}\right\}ds \\ &= \frac{\beta_g k}{\pi}K_0(\rho) + k\beta_g P(x, z, x_0, z_0),\end{aligned} \tag{47}$$

with $\rho = kR'$.

It is to be noticed that the values of P and its derivatives are exponentially decreasing with $k(z + z_0)$. So the corrective term P is essentially limited to a surface wave near the ground.

5. TEST FOR A POINT SOURCE IN A HALF-SPACE

The method is tested for a point source in a half-space without barrier because the 3D sound pressure can be calculated analytically. The 2D pressure is obtained for real and *imaginary* wavenumbers from the formulae (33), (56) and (40). Then the 3D pressure obtained by formula (16) is compared to the analytical solution for a point source over an impedance plane. An expression for the solution was obtained Thomasson [10] who derived the formula given in Appendix B. The purpose of this example is to test the accuracy of the method in this simple case. It is not intended to be competitive to the Thomasson solution in calculation cost for the half-space without barrier.

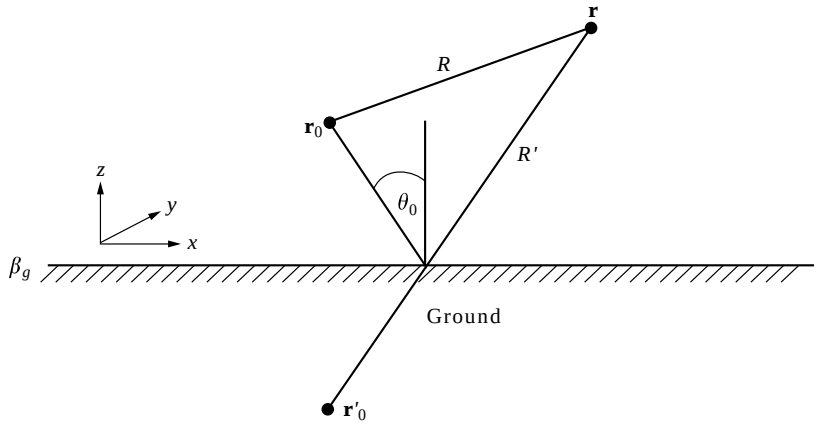

Figure 4. Source and reception points.

TABLE 1

Source and reception points

	x(m)	y(m)	z(m)
$\mathbf{r}_0$	0	0	0·5
$R1$	0·1	0	0·5
$R2$	10	10	2

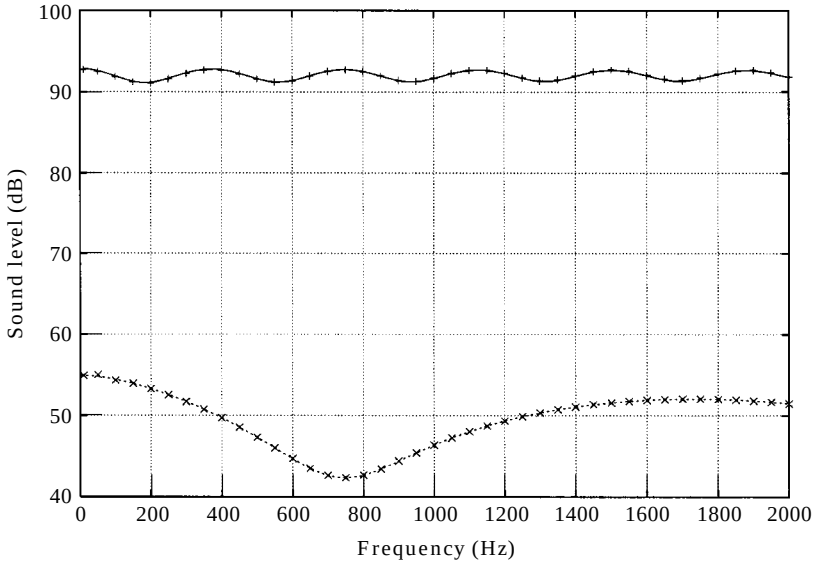

Figure 5. —, 3D solution point 1; + + +, 2D to 3D transform point 1; - - -, 3D solution point 2; × × ×, 2D to 3D transform point 2.

The source and reception points are shown in Figure 4. The source position has been chosen at 50 cm high with the co-ordinates given in Table 1. Two reception points were chosen where the pressure has been calculated over the frequency band [0, 2000 Hz]. The co-ordinates of these points are given in Table 1. The point $R1$

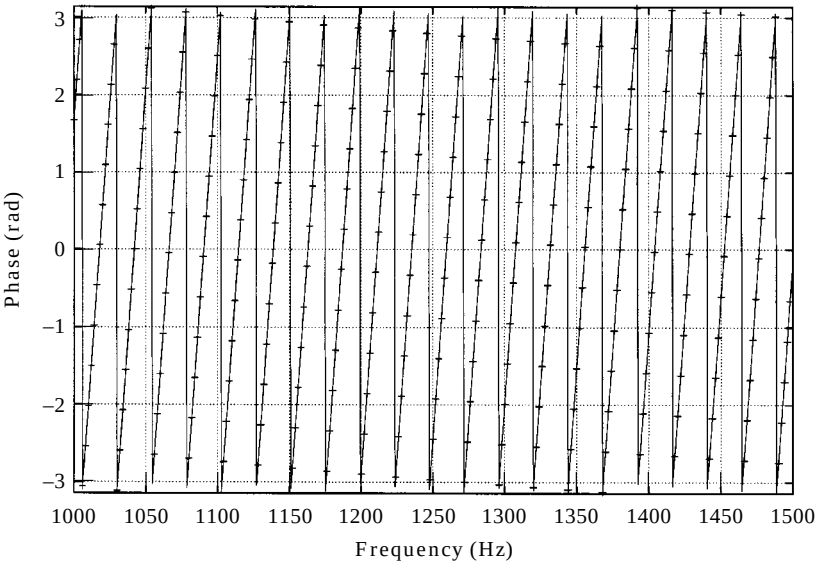

Figure 6. Phase of the presure at point 2. —, 3D solution; + + +, 2D to 3D transform

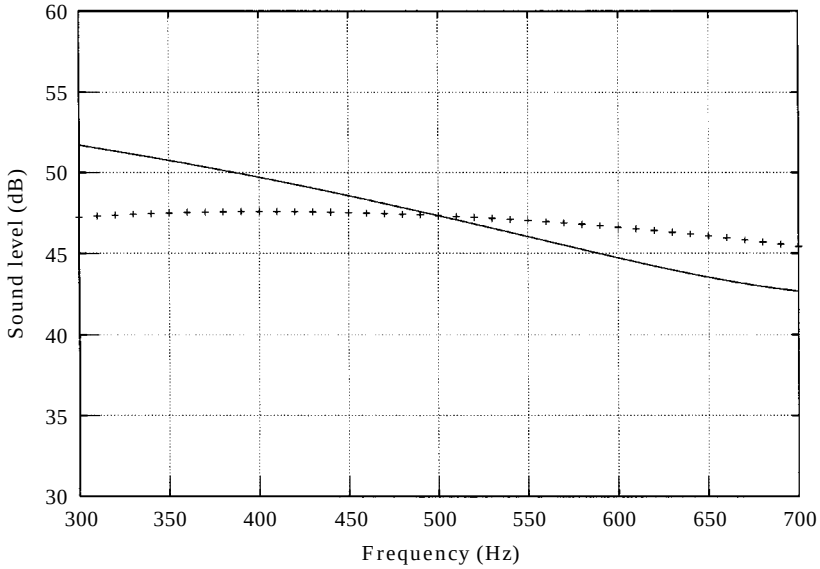

Figure 7. Transformation of 2D solutions calculated for $F = 500$ Hz (sound level). —, 3D solution; $+++$, 2D to 3D transform.

is very close to the source while the point $R2$ is further and not in the x–z plan. The normalized admittance β_g is given by the Delany and Bazley [21] formula

$$\frac{1}{\beta_g} = 1 + 9{\cdot}08\left(\frac{1000f}{\sigma}\right)^{-0{\cdot}75} + 11{\cdot}9\mathrm{i}\left(\frac{1000f}{\sigma}\right)^{-0{\cdot}73}, \tag{48}$$

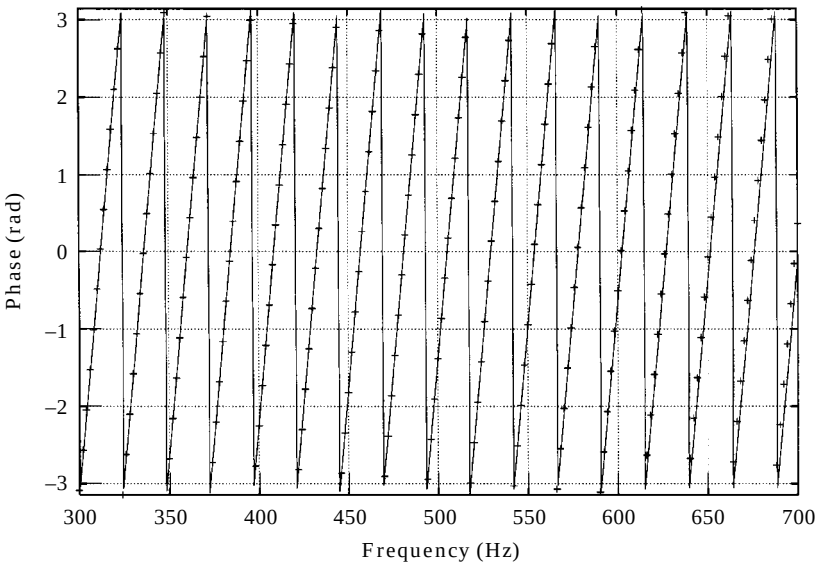

Figure 8. Transformation of 2D solutions calculated for $F = 500$ Hz (phase of the pressure). —, 3D solution; $+++$, 2D to 3D transform.

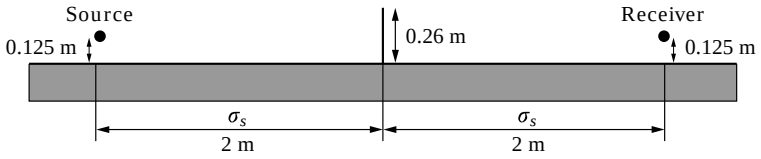

Figure 9. Scale model geometry.

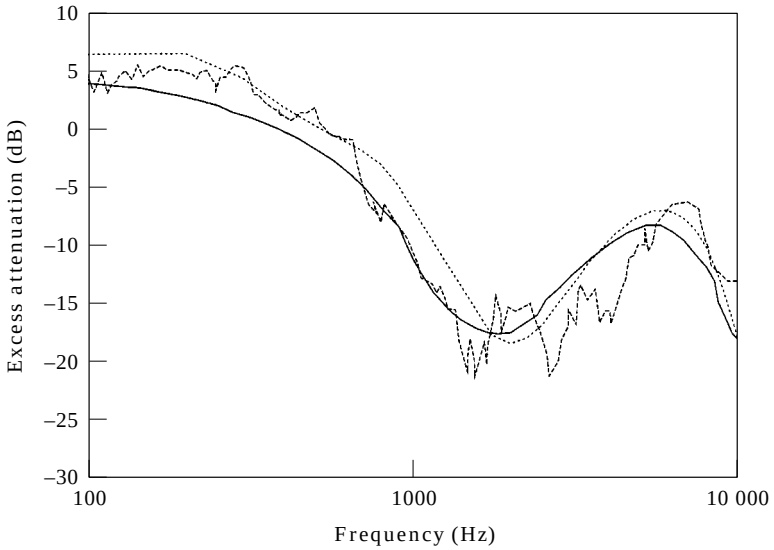

Figure 10. Comparison with reference [12] (Figure 5c) results. —, Ray method; - - -, measurement; . . . , BEM result.

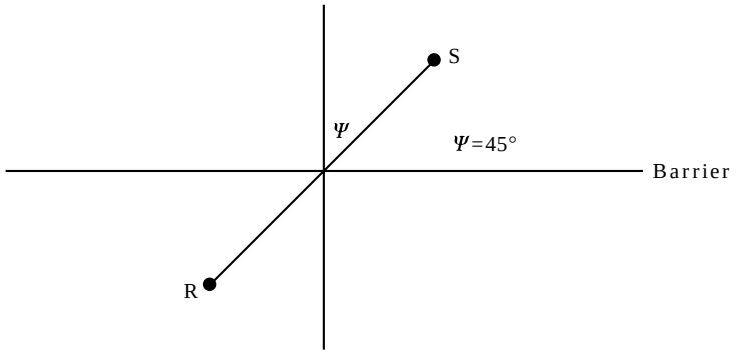

Figure 11. Source and receiver points.

where f is the frequency in Hertz and σ the flow resistance in SI unit. For these examples the flow resistance σ is equal to 300×10^3 Ns/m^4 which is a usual value for a grass surface. The sound speed is $c = 345$ m/s.

For every 3D frequency F the two-dimensional solutions q have been calculated for discrete 2D frequencies f in the interval $[0, F]$ and in the imaginary interval $[0, 2000 * i]$ with a 5-Hz step between two frequency points. Then the 2D to 3D transformation was calculated by formula (16). The 2D solution was constructed by quadratic interpolation from the precedent discrete values. Further details on numerical aspects can be found in references [6, 7].

In Figures 5 and 6 are presented the sound level and the phase of the pressure for the points $R1$ and $R2$ calculated by the 2D to 3D transformation and the pressure obtained from the 3D solution (59). In each case the two solutions are very close. At point $R1$ the pressure is high and the phase has low oscillations because of the proximity of the sound source. At point $R2$ the large distance creates strong oscillations in the phase but the comparison is still very good. To avoid an overcomplicated figure at this point the phase is only presented in the frequency range [1000 Hz, 1500 Hz]. It was observed that the modulus and the phase of the pressure are calculated accurately.

The main difference between a rigid and an impedance boundary is the need for a new set of 2D calculations for each 3D frequency. One can ask however if a 2D solution set calculated for a 3D frequency can be used for neighbouring 3D frequencies. To test this hypothesis a calculation of the 2D solutions set corresponding to the 3D frequency 500 Hz was made, then this set was used to build the 3D pressure over the frequency band [300 Hz, 700 Hz]. The results are presented in Figures 7 and 8 for the point $R2$. The phase of the pressure seems correctly evaluated over a large frequency range. On the contrary the modulus is well estimated on a small frequency range. Consequently it seems better to recalculate the 2D solution set for each 3D frequency.

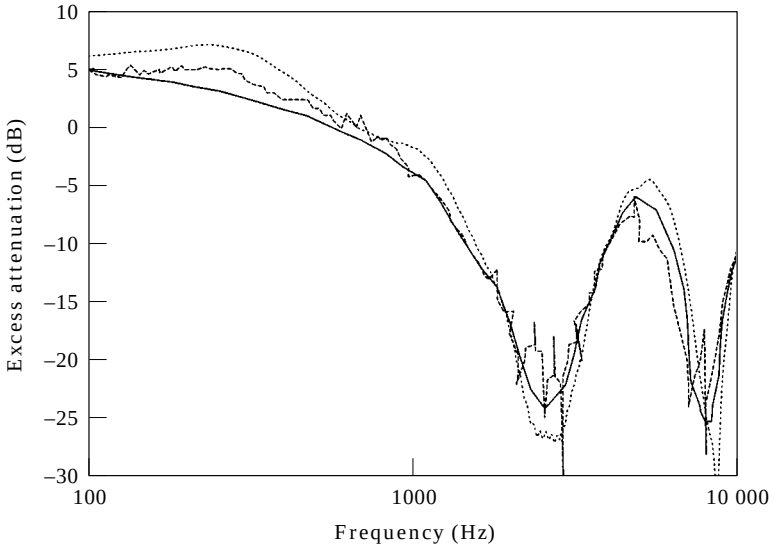

Figure 12. Angle 45°. —, Ray method; - - - , measurement; . . . , BEM result.

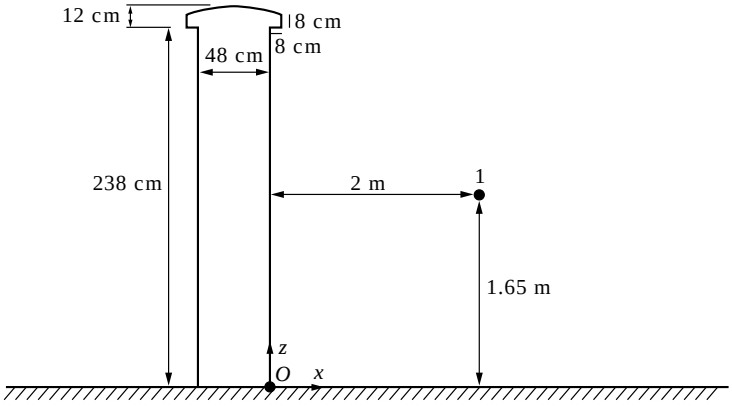

Figure 13. Cross-section of the barrier.

6. EXPERIMENTAL AND NUMERICAL RESULTS

6.1. SCALE MODEL

First, the results are compared to the numerical and scale model experiments presented by Isei *et al*. [22]. The geometry is shown in Figure 9 and consists of a rigid barrier on an impedance ground with $\sigma_s = 300\,000$ Ns/m^4. The excess attenuation, defined as the sound level with barrier relative to the sound level in free space, is presented in Figure 10. Our results are similar to both the measurements and the anlytical results obtained by a ray method.

Then, another comparison is made in the case of a rigid ground for the angle of incidence 45°. The source and the receiver are now separated by a distance of 2 m with the barrier symmetrically located between them (see Figure 11). Figure 12 gives the excess attenuation and comparisons are made with measurement results and ray calculations taken from Figure 9 of reference [22]. The present results compare favourably with those of reference [22]. However, the present results are not as accurate as the ray method in this case since for simple geometry the ray method does provide very accurate results. For practical applications the method presented here should be used for complex shapes where multiple reflections occurs. In such cases the ray method may be less accurate [23].

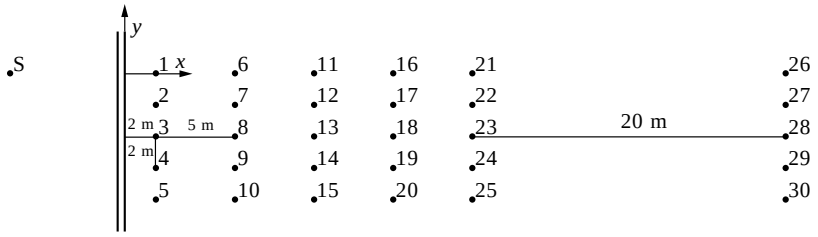

Figure 14. Measurement points.

Sp					
–0.1	–0.2	–1.5	–0.6	0.0	0.4
0.0	1.5	–0.3	–0.9	0.2	0.7
–1.7	2.5	–0.1	–0.2	0.3	–0.1
–1.2	1.2	–0.0	–0.3	1.0	0.4
–0.9	0.0	–1.1	–0.8	1.1	0.6

Figure 15. Difference between measurement and calculus at 125 Hz.

Sp					
–0.7	0.7	2.2	1.4	–0.5	1.5
–3.6	–0.9	0.9	1.0	–1.4	0.1
1.3	–0.3	1.6	1.0	–1.7	–1.4
–2.0	–0.2	1.6	0.0	–2.4	–1.9
2.4	0.4	2.9	0.7	–2.1	–0.4

Figure 16. Difference between measurement and calculus at 250 Hz.

Sp					
1.3	0.0	–0.4	–2.0	0.1	1.3
1.6	1.6	0.0	–2.4	1.2	1.5
3.0	0.8	1.0	–2.9	1.0	1.2
0.1	–2.1	0.7	–0.5	0.7	–1.2
–5.8	–0.8	–1.5	0.9	3.0	–1.5

Figure 17. Difference between measurement and calculus at 500 Hz.

Sp					
1.6	2.5	0.6	2.0	2.3	–0.7
0.9	–0.0	–1.6	–0.2	2.5	0.6
–2.4	0.6	–1.6	–1.8	–0.6	0.8
1.1	0.6	–0.6	0.3	0.1	0.7
–3.5	–2.6	–0.7	–0.7	1.0	–1.9

Figure 18. Difference between measurement and calculus at 1000 Hz.

6.2. FULL SCALE EXPERIMENT

To estimate the ability of these calculations to evaluate real sound pressures, an experiment was also conducted outdoors in the vicinity of a noise barrier. The barrier had uniform cross-section and was located between two fields in a quiet zone. The ground was of the same type on both sides of the barrier and consisted of earth without vegetation. The wall was made of stones binded with mortar and considered as rigid in the calculation. Although this is only an approximation, some calculations with impedance boundary conditions have shown that this effect was much less important than the ground properties. The cross-section is shown

TABLE 2

Average error e in dB

	125 Hz	250 Hz	500 Hz	1000 Hz
Rigid ground	1·0	4·8	3·7	4·5
$\sigma = 100\,000$ Ns/m^4	0·7	1·3	1·4	1·2

in Figure 13 and the origin of the co-ordinates is placed at the right bottom of the barrier.

The signal created by a signal generator, is then amplified by a 350-W power amplifier and finally sent to the sound source which is a loudspeaker located at point $(-7{\cdot}12, 0, 0{\cdot}3)$. It is approximated by a point source with no directivity. Measurements were made for harmonic noise at octave center frequencies.

The sound pressure is measured at 30 points in the shadow zone. These points are shown in Figure 14. The furthest point is 42 m from the barrier and the nearest is 2 m. All points are at the same level $z = 1{\cdot}65$ m above the ground. The sound level is measured with a Larson Davis microphone linked to a spectral analyzer. The sound level at the frequencies of interest was obtained in dB for each measurement point.

Sound pressure measurements in a half-space far from the barrier allowed a calculation for $\sigma = 100\,000$ Ns/m^4 as the best estimate for the ground parameter of the Delany and Bazley model. The numerical results are calculated using the 2D BEM with this value for σ and with an inter-node spacing of $\lambda/10$ to all precise solutions. Then the 2D to 3D transformation gives the three-dimensional sound

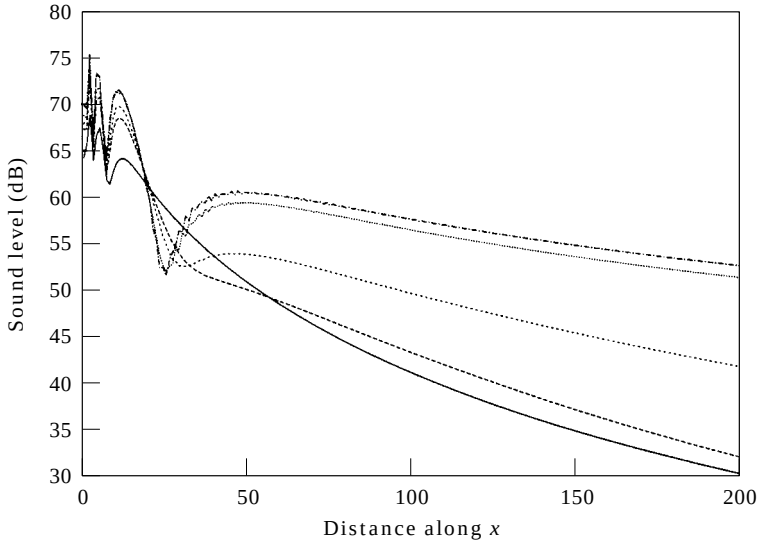

Figure 19. Sound level along x. —, $\sigma = 100 \times 10^3$; – – –, $\sigma = 500 \times 10^3$; - - -, $\sigma = 1000 \times 10^3$; . . . , $\sigma = 1000 \times 10^3$; – · –, $\sigma = \infty$.

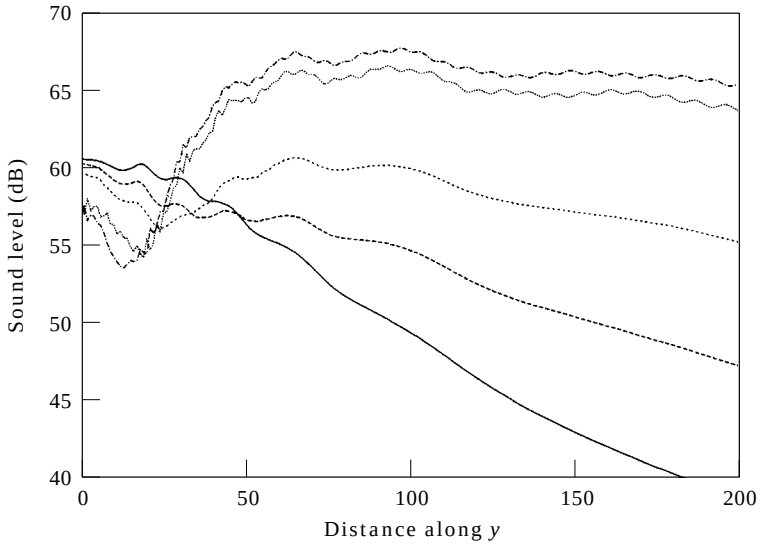

Figure 20. As Figure 19 but along y.

pressure. As the source amplitude is not known, the numerical results were first calculated for a unit point source only allowing an estimate of the relative sound level between two points. To be able to compare the calculated and measurement results, one has to shift the calculated values by a global sound level constant for each point. This constant, denoted L_g, is selected to minimize the error between the BEM model and the experimental results which is defined by

$$E = \sum_{i=1}^{i=30} [L_{cal}(i) + L_g - L_{mes}(i)]^2, \tag{49}$$

where $L_{mes}(i)$ is the measured sound level at point i and $L_{cal}(i)$ is the value calculated for a unit source. As there is only a single degree of freedom through the parameter L_g to estimate the sound level at 30 points, it is expected that the different errors will lead to $E > 0$. The minimal value of E after selection of the optimal L_g can provide an estimate of the quality of the model and of the experimental errors.

Measurements were made for harmonic sound pressures at frequencies 125, 250, 500 and 1000 Hz and at the points shown in Figure 14. Results are presented in Figures 15–18 where the difference between calculated and measured sound pressure are given at every point for the four frequencies. The measurement errors are of the order of 1 dB except at a few points where errors increase slightly. These errors come from atmospheric effects, errors in source and measurement point positions, the insufficiencies in the Delany and Bazley model, the non-homogeneities in the ground and the directivity of the source, amongst others.

To estimate the improvement brought by the impedance model over the rigid boundary condition, the averaged is calculated by the formula

$$e = \frac{1}{30} \sum_{i=1}^{i=30} |L_{cal}(i) + L_g - L_{mes}(i)|. \tag{50}$$

Here $L_{cal}(i) + L_g$ is the calculated value after shifting of the global level by L_g and L_{mes} is the measured sound level. Two series of calculations are made. The first one is for $\sigma = 100\,000$ Ns/m^4 and the second one for a rigid ground. In each case a different value of L_g is selected as the one which minimizes the value of E given by formula (49). The results are presented in Table 2. The model with a rigid ground leads to an error of about 4 dB while taking into account the impedance boundary condition reduces this error to less than 1·5 dB.

Finally, to compare the rigid and impedance grounds, the sound pressure has been calculated for the frequency 500 Hz along the x-axis for the points (x, 0, 1·65) with $1 \leqslant x \leqslant 200$ and along y for the points (22, y, 1·65) with $0 \leqslant y \leqslant 200$. The sound level at point (2, 0, 1·65) is taken equal to the measured value for $\sigma = 100 \times 10^3$. Figures 19 and 20 show the results along x and y, respectively. The impedance of the ground has a limited effect near the barrier but is very important for long range propagation. This is mainly true in the y direction where the sound pressure decreases very slowly for rigid ground.

7. CONCLUSION

A method is presented for calculating the sound pressure around noise barriers with uniform cross-section. The calculations give modulus and phase of the pressure solution of the three-dimensional Helmholtz equation with a point source excitation. It is able to take into account an impedance boundary condition on the groun and on the barrier. Comparisons with experimental data have shown an agreement with calculated values with an error of order 1·5 dB. Comparisons with ray methods for simple geometries show that the ray method gives accurate results in such cases. The method presented here should be used for complex shapes for which the ray method may be less accurate.

ACKNOWLEDGMENTS

The authors gratefully acknowledge the anonymous referees for their suggestions to improve this paper.

REFERENCES

1. R. Seznec 1980 *Journal of Sound and Vibration* **73**, 195–209. Diffraction of sound around barriers: use of the boundary elements technique.
2. D. C. Hothersall, S. N. Chandler-Wilde and M. N. Hajmirzae 1991 *Journal of Sound and Vibration* **146**, 303–322. Efficiency of single noise barriers.
3. D. C. Hothersall, D. H. Crombie and S. N. Chandler-Wilde 1991 *Applied Acoustics* **32**, 269–287. The performance of T-profile and associated noise barriers.

4. Y. KAWAI and T. TERAI 1990 *Applied Acoustics* **31** 101–117. The application of integral equation methods to the calculation of sound attenuation by barriers.
5. H. ANTES 1991 In *Boundary Element Methods in Acoustics*, 225–260, chap. 11. Computational mechanics publications. Amsterdam: Elsevier Applied Sciences. Applications in environmental noise.
6. D. DUHAMEL 1994 *PhD thesis*, *Ecole Nationale des Ponts et Chaussées*. L'acoustique des problèmes couplés fluide-structure: application au contrôle actif du son.
7. D. DUHAMEL 1996 *Journal of Sound and Vibration* **197**, 547–571. Efficient calculation of the three-dimensional sound pressure field around a noise barrier.
8. U. INGARD 1951 *Journal of the Acoustical Society of America* **23**, 329–335. On the reflection of a spherical sound wave from an infinite plane.
9. A. R. WENZEL 1974 *Journal of the Acoustical Society of America* **55**, 956–963. Propagation of waves along an impedance boundary.
10. S. I. THOMASSON 1976 *Journal of the Acoustical Society of America* **59**, 780–785. Reflection of waves from a point source by an impedance boundary.
11. C. F. CHIEN and W. W. SOROKA 1975 *Journal of Sound and Vibration* **43**, 9–20. Sound propagation along an impedance plane.
12. C. F. CHIEN and W. W. SOROKA 1980 *Journal of Sound and Vibration* **69**, 340–343. A note on the calculation of sound propagation along an impedance plane.
13. S. I. THOMASSON 1980 *Acustica* **45**, 122–125. A powerful asymptotic solution for sound propagation above an impedance boundary.
14. T. KAWAI, T. HIDAKA and T. NAKAJIMA 1982 *Journal of Sound and Vibration* **83**, 125–138. Sound propagation above an impedance boundary.
15. M. A. NOBILE and S. I. HAYEK 1985 *Journal of the Acoustical Society of America* **78**, 1325–1336. Acoustic propagation over an impedance plane.
16. Y. L. LI, M. J. WHITE and M. H. HWANG 1994 *Journal of the Acoustical Society of America* **96**, 2485–2490. Green's functions for wave propagation above an impedance ground.
17. S. N. CHANDLER-WILDE and D. C. HOTHERSALL 1985 *Journal of Sound and Vibration* **98**, 475–491. Sound propagation above an inhomogeneous impedance plane.
18. S. N. CHANDLER-WILDE and D. C. HOTHERSALL 1995 *Journal of Sound and Vibration* **180**, 705–724. Efficient calculation of the Green function for acoustic propagation above a homogeneous impedance plane.
19. I. S. GRADSHTEYN and I. M. RYZHIK 1980 *Table of Integrals*, *Series and Products*. New York: Academic Press.
20. C. H. WILCOX 1975 volume 442 of Lecture Notes in Mathematics. Berlin: Spriger-Verlag *Scattering Theory for the d'Alembert Equation in Exterior Domains*.
21. M. E. DELANY and E. N. BAZLEY 1970 *Applied Acoustics* **3**, 105–116. Acoustical properties of fibrous absorbent materials.
22. T. ISEI, T. F. W. EMBLETON and J. E. PIERCY 1980 *Journal of the Acoustical Society of America* **67**, 46–58. Noise reduction by barriers on finite impedance ground.
23. E. M. SALOMONS, A. C. GEERLINGS and D. DUHAMEL 1997 *Acta Acustica* **83**, 35–47. Comparison of a ray model and a Fourier-boundary element method for traffic noise situations with multiple diffractions and reflections.

APPENDIX A: CORRECTIVE TERM IN THE GREEN FUNCTION

The Green function with an admittance boundary condition on the ground is written as

$$G(\mathbf{r}, \mathbf{r}_0) = G_0(\mathbf{r}, \mathbf{r}_0) + P(\mathbf{r}, \mathbf{r}_0). \tag{A1}$$

The corrective term $P(\mathbf{r}, \mathbf{r}_0)$ is the solution

$$\Delta P(\mathbf{r}, \mathbf{r}_0) + k^2 P(\mathbf{r}, \mathbf{r}_0) = 0, \tag{A2}$$

$$\frac{\partial P}{\partial z}(\mathbf{r}, \mathbf{r}_0) + \mathrm{i}k\beta_g P(\mathbf{r}, \mathbf{r}_0) = \frac{k\beta_g}{2} \mathrm{H}_0^{(1)}(kR) \quad \text{on} \quad S_2, \tag{A3}$$

$$\frac{\partial P}{\partial n}(\mathbf{r}, \mathbf{r}_0) - \mathrm{i}kP(\mathbf{r}, \mathbf{r}_0) = o\left(\frac{1}{\sqrt{r}}\right), \tag{A4}$$

$$P(\mathbf{r}, \mathbf{r}_0) = o\left(\frac{1}{\sqrt{r}}\right). \tag{A5}$$

P can be calculated by taking a Fourier transform along x, solving the differential equation in the variable z satisfied by the Fourier transform and then taking the inverse Fourier transform. Details can be found in reference [18] and only the final expressions are given here. P is calculated by

$$P(\mathbf{r}, \mathbf{r}_0) = -\frac{\mathrm{i}\beta_g}{2\pi} \int_{-\infty}^{+\infty} \frac{\mathrm{e}^{\mathrm{i}k((z+z_0)\sqrt{1-s^2} - (x-x_0)s)}}{\sqrt{1-s^2}(\sqrt{1-s^2} + \beta_g)} \, \mathrm{d}s. \tag{A6}$$

The precedent formula is not well adapted to numerical integrations because of the rapid oscillations in the integrand. Chandler-Wilde and Hothersall [18] proved that P can be more efficiently calculated by the following formula

$$P(\mathbf{r}, \mathbf{r}_0) = -\frac{\beta_g \, \mathrm{e}^{\mathrm{i}\rho}}{\pi} \int_0^{+\infty} \frac{\mathrm{e}^{-\rho t}}{\sqrt{t}} g(t) \, \mathrm{d}t - \frac{\beta_g \, \mathrm{e}^{\mathrm{i}\rho(1-a_+)}}{2\sqrt{1-\beta_g^2}} \operatorname{erfc}(\mathrm{e}^{-\mathrm{i}\pi/4}\sqrt{\rho}\sqrt{a_+}), \tag{A7}$$

where

$$\begin{aligned}
g(t) &= f(t) - \mathrm{e}^{-\mathrm{i}\pi/4}\sqrt{a_+}/\{2\sqrt{1-\beta_g^2}(t - \mathrm{i}a_+)\}, \\
f(t) &= -\frac{(\beta_g + \gamma(1 + \mathrm{i}t))}{\sqrt{t - 2\mathrm{i}}(t^2 - 2\mathrm{i}(1 + \beta_g\gamma)t - (\beta_g + \gamma)^2)}, \\
a_+ &= 1 + \beta_g\gamma - \sqrt{1-\beta_g^2}\sqrt{1-\gamma^2}, \\
\gamma &= (z + z_0)/R', \\
\rho &= kR', \\
\mathrm{Re}\{\sqrt{a_+}\}, &\quad \mathrm{Re}\{\sqrt{1-\beta_g^2}\}, \quad \mathrm{Re}\{\sqrt{t-2\mathrm{i}}\} \geqslant 0,
\end{aligned} \tag{A8}$$

and erfc is the complementary error function. It is proved that $g(t)$ is regular in $\mathrm{Im}\,(t) < 1$ so the integration of g can be evaluated numerically.

APPENDIX B: POINT SOURCE ABOVE AN IMPEDANCE PLANE

Thomasson [10] obtained the following formulae for the sound pressure of a point source above an impedance plane

$$G(\mathbf{r}, \mathbf{r}_0) = \frac{\mathrm{e}^{\mathrm{i}KR}}{4\pi R} + \frac{\mathrm{e}^{\mathrm{i}KR'}}{4\pi R'} - P, \tag{B1}$$

$$P = \begin{cases} P_{SD} + PB & \text{when} \quad \mathrm{Re}\,(a_+) < 0 \quad \text{and} \quad \mathrm{Im}\,(\beta_g) < 0 \\ P_{SD} & \text{else} \end{cases}, \tag{B2}$$

where

$$P_B = \frac{K\beta_g}{2}\,\mathrm{H}_0^{(1)}[KR(1-\beta_g^2)^{1/2}]\,\mathrm{e}^{-\mathrm{i}K(z+z_0)\beta_g}, \tag{B3}$$

$$P_{SD} = \frac{K\beta_g}{2\pi}\,\mathrm{e}^{\mathrm{i}KR'} I, \tag{B4}$$

$$I = \int_0^{+\infty} \frac{\mathrm{e}^{-KR't}}{W^{1/2}(t)}\,\mathrm{d}t, \tag{B5}$$

and

$$W(t) = [\cos(\theta_0) + \beta_g]^2 + 2\mathrm{i}t[1 + \cos(\theta_0)\beta_g] - t^2,$$

$$t_1 = -\mathrm{Im}\,(\beta_g)[\mathrm{Re}\,(\beta_g) + \cos(\theta_0)]/[1 + \cos(\theta_0)\,\mathrm{Re}\,(\beta_g)],$$

$$a_+ = 1 + \beta_g \cos(\theta_0) - (1-\beta_g^2)^{1/2} \sin(\theta_0),$$

$$\cos(\theta_0) = (z + z_0)/R',$$

$$\sin(\theta_0) = ((x - x_0)^2 + (y - y_0)^2)^{1/2}/R',$$

$$\mathrm{Re}\,\{(1 - \beta_g^2)^{1/2}\} > 0,$$

$$\mathrm{Re}\,(W^{1/2}) \begin{cases} < 0 & \text{when} \quad \mathrm{Re}\,(a_+) < 0, \quad \mathrm{Im}\,(\beta_g) < 0 \quad \text{and} \quad t > t_1 \\ > 0 & \text{else} \end{cases}. \tag{B6}$$